https://doi.org/10.48047/AFJBS.6.15.2024.11034-11043

African Journal of Biological Sciences

Journal homepage: http://www.afjbs.com

Research Paper Open Access

Investigating the Structural, Electronic, and Optical Characteristics of Bulk andMonolayer CrSe

Ammar A. Kadhim [a,b], H Sedghi [a], Jabbar M. Khalaf Al-zyadi [b]

a Department of Physics, Faculty of Science, Urmia University, Urmia, Iran
b Department of Physics, College of Education for Pure Sciences, University of Basrah, Basrah,Iraq

*__Corresponding Author__:
E-mail addresses: a.abduljabbar@urmia.ac.ir & ammar.kadhim@uobasrah.edu.iq (Ammar A. Kadhim).
h.sedghi@urmia.ac.ir (H Sedghi).
jabbar.khalaf@uobasrah.edu.iq, jabbar_alzyadi@yahoo.com (J.M. Khalaf Al-zyadi).

Volume 6, Issue 15, Sep 2024

Received: 15 July 2024

Accepted: 25 Aug 2024

Published: 25 Sep 2024

doi: 10.48047/AFJBS.6.15.2024.11034-11043

Abstract
This paper presents a detailed investigation of the electronic and optical properties of CrSe in both bulk and monolayer forms, using the ab initio method. Since half metals and spin-gapless semiconductors show complete (100%) electron spin polarization around the Fermi level, they are interesting candidates for spintronic applications. The first-principles calculations used in this research focused on the electronic, optical, and elastic properties of CrSe, a binary Heusler alloy. Our analysis of the elastic constants revealed that the alloy is mechanically stable. Our electronic and magnetic properties analysis revealed that the alloy is a half-metallic (HM) ferrimagnet with a total magnetic moment (Mtot) of 4 μB/ f.u. The optimized lattice constants for the bulk and monolayer forms were 4.12 Å and 3.54 Å, respectively, and satisfy the Slater-Pauling rule (Mt=Zt- 8). Additionally, we calculated the optical spectra of the alloy in the range of energy 0-15 eV, including the actual and imaginary portions of the dielectric function, and absorption coefficient.

Keywords: Half-metallic; Electronic structures; Magnetic properties; First-principles.ferromagnetic.

Introduction

Thanks to an electron's intrinsic spin property, which complements its charge [1,2], the field of spintronics has witnessed remarkable growth in the past decade. This emerging topic has stimulated fundamental interest and technological developments, such as the creation of non-volatile magnetic random-access memory (MRAMs), magnetoresistive devices, and the concept of self-assembled quantum computers [3]. The need to introduce a highly spin-polarized current from magnetic materials into semiconductors is a major challenge in spintronics [4].

Half-metallic ferromagnetic has emerged as a novel class of materials due to their extraordinary characteristics. They exhibit metallic behavior in one spin channel, while the other spin direction manifests a band gap at the Fermi level, endowing it with semiconducting attributes [5]. In high-performance spintronics applications, this family of materials is essential, especially as a source of spin-polarized carriers that may be injected into semiconductor devices. Theoretically, achieving 100% spin polarization at the Fermi surface is imperative for optimal functionality [6,7].

Ternary half-Heusler alloys are generally represented by the generic formulas XYZ and X2YZ, respectively. The XYZ composition half-Heusler alloys are categorized in space group F43m (No. 216) and have a face-centered cubic Clb structure. The X, Y, and Z components occupy the 4a (0, 0, 0), 4c (1/4, 1/4, 1/4), and 4d (3/4, 3/4, 3/4) Wyckoff places in this structure, respectively.

The full-Heusler alloys, known as X2YZ, on the other hand, can adopt either the Cu2MnAl-type or the Hg2CuTi-type structure. The elements X, X, Y, and Z are found in the Hg2CuTi-type structure, which is also found in space group F43m (No. 216), at the Wyckoff positions 4a (0, 0, 0), 4c (1/4, 1/4, 1/4), 4b (1/2, 1/2, 1/2), and 4d (3/4, 3/4, 3/4). Conversely, the following Wyckoff positions correspond to the components X, Y, Z, and Cu2MnAl-type structure with space group Fm3m (No. 225): 4a (0, 0, 0), 4c (1/4, 1/4, 1/4), 4b (1/2, 1/2, 1/2), and 4d (3/4, 3/4, 3/4).

In half-Heusler alloys, researchers have delved into the investigation of their half-metallic properties through a combination of theoretical modeling and experimental analysis. The pioneering discovery of a half-metallic material was made with NiMnSb [8]. Subsequently, a roster of other intriguing alloys, including PtMnSb, NiCrZ, and MnCrSb [9–13], have been documented in the literature.

A noteworthy recent development comes from Fujii et al., who reported the emergence of half-metallicity in binary alloys Mn2Z (where Z represents P, As, Sb, or Ge) featuring the distinctive half-Heusler crystal structure [14]. Meanwhile, Luo et al. unveiled Mn2Sn as a unique half-metallic fully compensated ferrimagnet (HMFCF) [15], characterized by a delicate balance of magnetic moments at the A and B sites that effectively cancel each other out, resulting in a net zero total moment.

Furthermore, it is worth noting that in the case of Mn2Sn, a transition from a half-metallic state to a semi-metallic state has been predicted to occur under the influence of external pressure, adding an intriguing dimension to the study of these materials.

If we exclude the Y atom, the ternary full-Heusler alloys X2YZ can be simplified to binary Heusler alloys X2Z and XZ. In recent times, binary Heusler alloys have garnered increased attention, surpassing their previous level of popularity. Notably, binary Heusler alloys such as Fe2Z (Z=In, Sn, Sb, As) [16] and Mn2Sn [17, 18] have been found to exhibit intriguing half-metallic (HM) characteristics through rigorous first-principles calculations. Motivated by these findings, our study delves into the investigation of the structural, electronic, magnetic, and elastic properties of the binary Heusler alloy CrSe.

Our examination of the band structure and magnetic moment is driven by the goal of assessing the suitability of the CrSe monolayer as a material for spintronic devices. Encouragingly, our findings suggest that the CrSe monolayer exhibits substantial potential as a prime candidate for 2D spintronic applications.

1. Computational Method

To analyze the structural, electronic, magnetic, and optical properties of CrSe, we employed density functional theory (DFT) as implemented in the CASTEP code [19]. The exchange-correlation energy was treated using the generalized gradient approximation (GGA) with the Perdew-Burke-Ernzerhof (PBE) formulation [20]. In our study, we focused on a monolayer of CrSe, which was constructed as a 6×6×1 supercell.

To eliminate any spurious interactions between periodic images along the vertical direction, we introduced an additional 15 Å spacing perpendicular to the 2D monolayer surface. The spin configuration of CrSe was carefully examined, and it was determined to be ferromagnetic, with all spins aligned either in the "up" or "down" direction, resulting in a non-zero magnetic moment.

A plane-wave basis set with a 300 eV cutoff energy was used for our computations. We set the threshold for overall energy convergence at 10-6 eV and relaxed all atomic positions until the atoms' forces were less than 0.01 eV/Å in order to ensure structural stability. We used a 15×15×1 k-mesh to sample the first Brillouin zone in order to precisely reproduce the characteristics of the CrSe monolayer. We have performed an accurate structural, electrical, magnetic, and optical property analysis of the CrSe monolayer using this comprehensive method.

2. Results and Discussion

2.1. Structural and electronic properties

The CrSe compound has a space group known as P-43m (216) and a cubic crystalline structure. In this configuration, the Cr and Se atoms are located in one formula unit at particular coordinates (0, 0, 0) for Cr and (0.25, 0.25, 0.25) for Se, as Figure 1 illustrates. The equilibrium lattice constants for both bulk and monolayer structures are 4.12 Å and 3.54 Å, respectively.

When the Heusler alloy model is applied to the band structure of CrSe in bulk and monolayer forms, different electronic behaviors are observed. Metallic characteristics are visible in the spin-majority channel, mainly because of bands that pass the Fermi level. On the other hand, the spin-minority channel has semiconductor properties with an indirect band gap between the largest valence band and the minimum conduction band. as illustrates In Figure 2.

Based on these findings, it can be said that CrSe materials, in both bulk and monolayer form, have half-metallic ferromagnet-like characteristics. In particular, an indirect band gap of 3.47 eV is observed in the bulk configuration of CrSe, whereas an indirect band gap of 2.57 eV is observed in the monolayer structure. The notion of the half-metallic gap (HMgap) is also presented; it is the smallest energy differential between the Fermi level and the minimum conduction band (MCB) or maximum valence band (MVB).

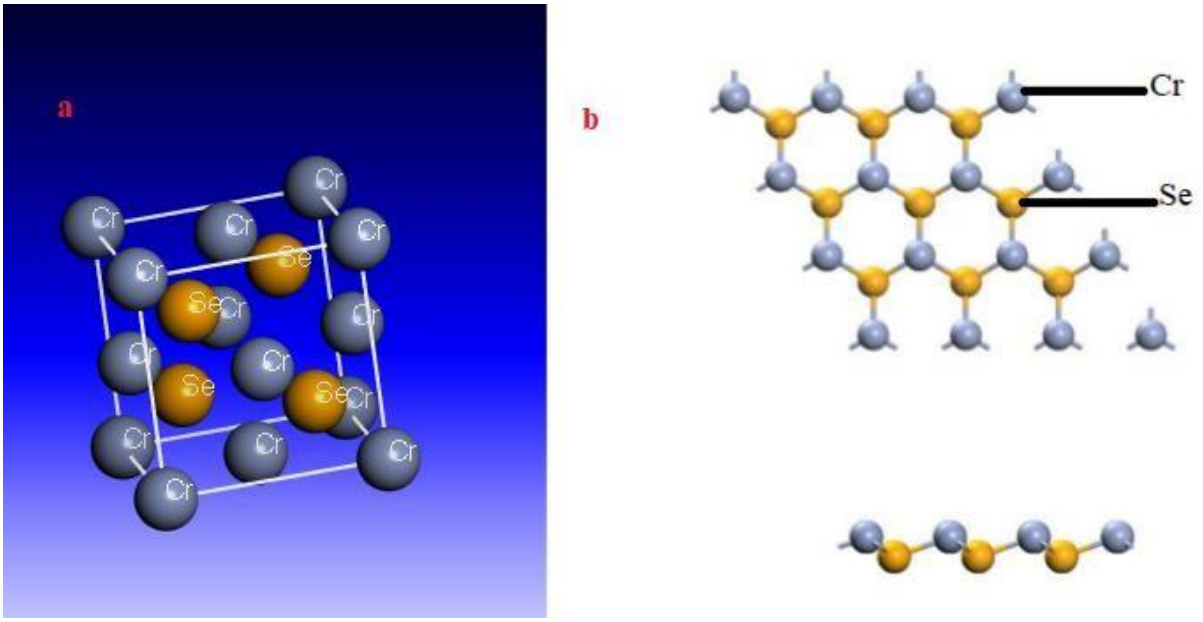

Figure 1 illustrates: (a) the crystal structure of bulk CrSe and (b) the atomic arrangement within the CrSe monolayer.

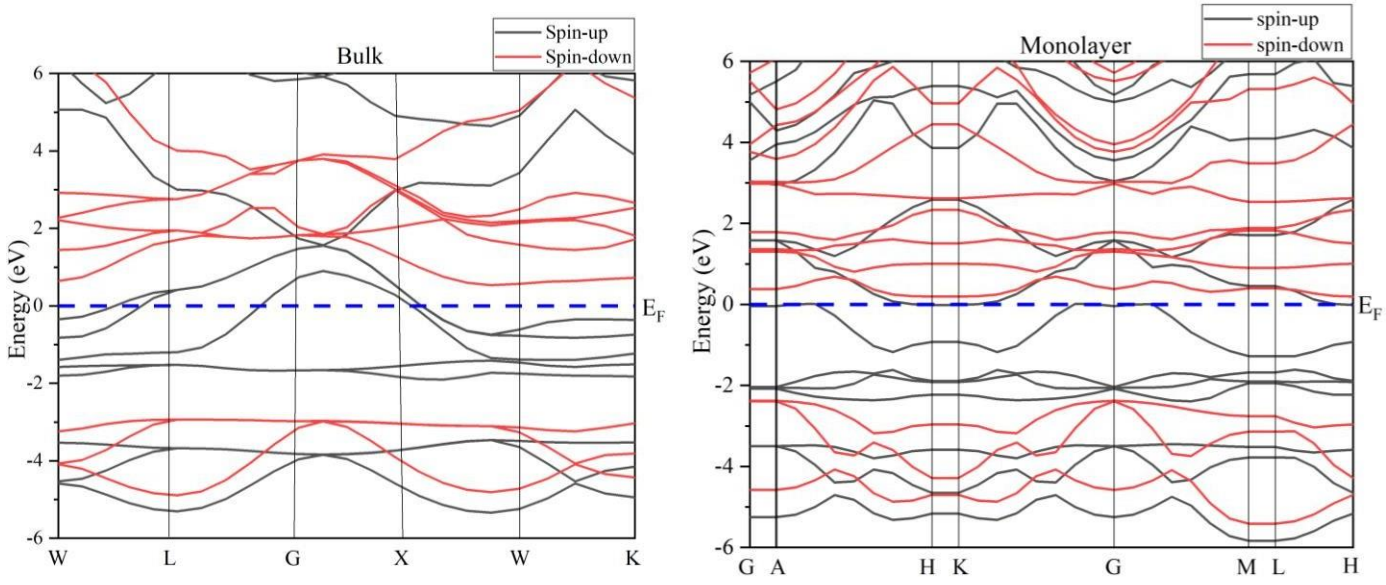

Figure 2 presents the band structures for both the bulk and monolayer configurations of CrSe.

2.2. The density of states and magnetic properties

For the half-Heusler alloy CrSe at its equilibrium lattice constant, we examined the total and partial density of states (TDOS and PDOS), as shown in Figure 3. The contributions of the Cr atom were the main source of the significant peak in the valence area of TDOS below the Fermi level, whereas

the contributions of the Se atom were relatively smaller. The Fermi energy level was set to zero and the spin-down state was multiplied by -1 to conform to convention.

On the other hand, a bandgap was evident in the minority spin DOS of the alloy, where Cr dominated the conduction band while Se states occupied the valence part of the DOS. In contrast, the DOS of the CrSe alloy and that of Cr and Se separately showed peaks at the Fermi energy level (EF) for the majority spin, showing that CrSe behaved metallically in this configuration. The fluctuations in the energy gap values corresponding to changes in the lattice parameter were also summarized in this study. Thus, we deduce that the hybridization of the Cr d-orbitals and the Se p-orbitals is responsible for the energy bandgap's appearance in CrSe.

Consequently, this mix of bulk and monolayer structures maintains its half-metallic (HM) property. Its large spin magnetic moment makes the Cr atom's significant contribution to the magnetic characteristics clear. This can be explained by the fact that the Cr atom has more electrons in its outermost electron shell than the other atoms do.

The Slater-Pauling formula [21, 22] can be used to find the total magnetic moment: $Mt = Zt-8$, where Zt is the total number of valence electrons in the primitive cell. The CrSe alloy has a total of 12 valence electrons when the valence electrons of Cr (4S13d5) and Se (4S24P4) are taken into account. Of the atoms, the Cr atom has the greatest effect on the total magnetic moment since it has a bigger spin magnetic moment than the other atoms. On the other hand, the Se atom has a relatively smaller contribution than the Cr atom.

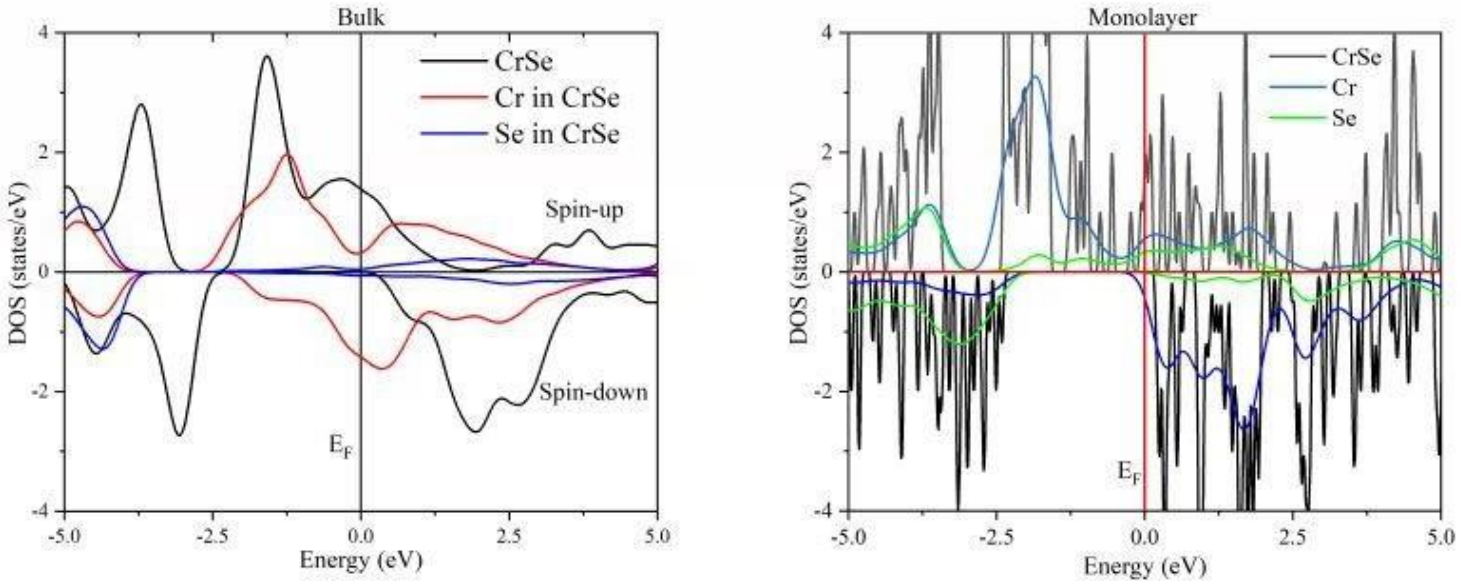

Figure 3 illustrates the partial and total density of states (DOS) for both bulk and monolayer CrSe.

2.3. Optical properties

The optical spectra of bulk and monolayer CrSe are depicted in Figure 4, illustrating their energy dependence. Our study focuses on the 0–15 eV energy range, crucial for understanding the optical properties of compounds in various applications and research contexts. To ensure precise computation of the complex dielectric function with self-energy and local field corrections, the FP-LAPW approach requires a dense grid and accurate exchange-correlation techniques. The Trans Blaha-Modified Becke-Johnson method proves to be an excellent choice for obtaining accurate optical property calculations when applied to a 30 × 30 × 30 grid. The results for the absorption coefficient A(ω)R(ω) and dielectric function ε(ω) are presented in this section.

The definition of the dielectric function ε(ω) is as follows:

$$\varepsilon(\omega) = \varepsilon_1(\omega) + i\varepsilon_2(\omega) \quad (1)$$

$$n(\omega) = \left[\frac{\sqrt{\varepsilon_1^2(\omega)+\varepsilon_2^2(\omega)+\varepsilon_1(\omega)}}{2}\right]^{1/2} \quad (2)$$

$$k(\omega) = \left[\frac{\sqrt{\varepsilon_1^2(\omega)+\varepsilon_2^2(\omega)-\varepsilon_1(\omega)}}{2}\right]^{1/2} \quad (3)$$

The dielectric function ε(ω) plots in Figure 4(c and d) show the relationship between photon energy and the dielectric function. Intra- and inter-band transitions contribute to the dielectric function. We analyze direct and indirect transitions in inter-band transitions, excluding indirect band gap excitation due to the lower photon momentum. The band structure influences the dielectric function, reflecting the material's response to an external electric field (E). Occupied and unoccupied wave functions from momentum matrix calculations primarily determine this function.

The dielectric function consists of two components: the imaginary part, ε2(ω), calculated by summing occupied-to-unoccupied transitions using the Fermi golden rule, and the real part, ε1(ω), which is linked to the propagative behavior of the electromagnetic field. The Kramer-Kronig relation is employed to determine the real part ε1(ω). The dielectric function of CrSe alloys in the photon energy range of 0–15 eV is depicted in Figure 4(c and d). Bulk CrSe has a static dielectric constant of 18.7, while monolayer CrSe has a static dielectric constant of 11.12. The value of ε1(0) remains relatively stable. The negative values of ε1(ω) indicate reflection of incident radiation on the surface. The real component of the dielectric constant for CrSe remains constant up to 15 eV. The optical band gap of the compound is equal to the imaginary component of the dielectric function's zero-frequency value, ε2.

We analyze the optical properties of bulk and monolayer CrSe by calculating the absorption coefficient A(ω). Both materials exhibit minimal absorption coefficients at energies below 0.0 eV, indicating a lack of electronic transitions. This is due to the photon energy being lower than the band gap of CrSe. However, as the energy approaches 15 eV, absorption features become more prominent, as shown in Figure 4(a) and (b). The maximum absorption coefficients for bulk and monolayer CrSe are 247,483 at 10.84 eV and 86,070 at 11.479 eV, respectively. These values demonstrate the wide band gap and strong ultraviolet absorption properties of CrSe, making it suitable for various applications, particularly in optoelectronic devices such as UV detectors.

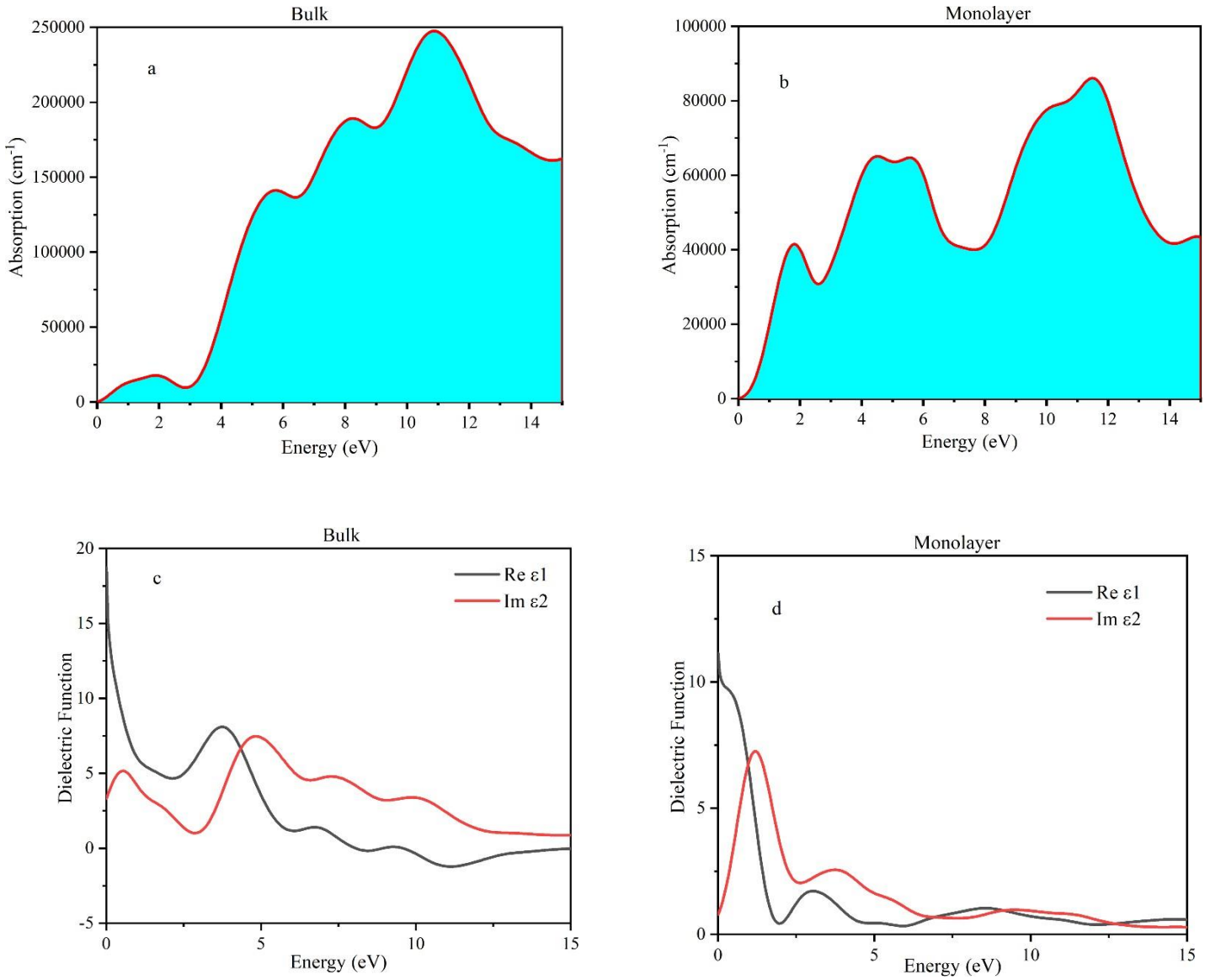

Figure 5 demonstrates the properties of bulk and monolayer CrSe. The absorption coefficient is shown in panels (a) and (b), while the real and imaginary components of the complex dielectric function are shown in panels (c) and (d), respectively.

Conflict of interest

The authors declare that there are no conflicts of interest.

References

[1] Prinz GA (1995) Spin-polarized transport. Phys Today 48:58 .https://doi.org/10.1063/1.881459.

[2] Kobayashi KI, Kimura T, Sawada H, Terakura K, Tokura Y. (1998) Room-temperature magnetoresistance in an oxide material with an ordered double-perovskite structure. Nature 395:677 e80 . https://doi.org/10.1038/27167.

[3] Bandyopadhyay S (2000) Self-assembled nanoelectronic quantum computer based on the Rashba effect in quantum dots. Phys Rev B 61:13813. https://doi.org/10.1103/PhysRevB.61.13813.

[4] Van Dorpe P, Motsnyi VF, Nijboer M, Goovaerts E, Safarov VI, Das J, et al. (2003) Highly efficient room temperature spin injection in a metal-insulator semiconductor light emitting diode. Jpn J Appl Phys 42:502e4. https://doi.org/10.48550/arXiv.cond-mat/0208325.

[5] De Groot R, Mueller F, Van Engen P, Buschow K (1983) New class of materials: half-metallic ferromagnets. Phys Rev Lett 50:2024e7. https://doi.org/10.1103/PhysRevLett.50.2024.

[6] Zutic I, Fabian J, Sarma SD (2004) Spintronics: fundamentals and applications. Rev Mod Phys 76:323. https://doi.org/10.1103/RevModPhys.76.323.

[7] Kübler J (2003) Curie temperatures of zinc-blende half-metallic ferromagnets. Phys Rev B 67:220403. https://doi.org/10.1103/PhysRevB.67.220403.

[8] de Groot R.A, Mueller F.M, Van Engen P.G, Buschow K.H.J (1983) Physical Review Letters 50-2024. https://doi.org/10.1103/PhysRevLett.50.2024.

[9] De Groot R.A, Mueller F.M, Van Engen P.G, Buschow K.H.J (1990) Journal of Applied Physics 55 2151. https://doi.org/10.1063/1.333593.

[10] S-as-ıoglu E, Sandratskii L.M, Bruno P (2005) Journal of Applied Physics 98 ˘063523. https://doi.org/10.1063/1.2060941.

[11] Nanda B.R.K, Dasgupta I (2006) Computational Materials Science 36 96. https://doi.org/10.1016/j.commatsci.2004.11.020.

[12] De Groot R.A (1991) Physica B 172, 45. https://doi.org/10.1016/0921-4526(91)90415-B.

[13] Casper F, Graf T, Chadov S, Balke B, Felser C (2012) Semiconductor Science and Technology 27, 063001. http://dx.doi.org/10.1088/0268-1242/27/6/063001.

[14] Fujii S, Ishida S, Asano S (2010) Journal of the Physical Society of Japan 79, 124702. https://doi.org/10.1143/JPSJ.79.124702.

[15] Luo H.Z, Liu G.D, Meng F.B, Wang W.H, Wu G.H, Zhu X.X, Jiang C.B (2011) Physica B 406, 4245. https://doi.org/10.1016/j.physb.2011.08.020.

[16] Li J Q, Meng F B, Liu G D, Chen X G, Luo H Z, Liu E and Wu G H (2013) Electronic structure and magnetism of binary Fe-based half-Heusler alloys Fe2Z (Z=In, Sn, Sb and As) J. Magn. Magn. Mater. 331, 82–87. https://doi.org/10.1016/j.jmmm.2012.11.038.

[17] Wang X T, Cheng Z X, Wang J L, and Liu G D (2016) A full spectrum of spintronic properties demonstrated by a C1b-type Heusler compound Mn2Sn subjected to strain engineering J. Mater. Chem. C 4 8535-8544. https://doi.org/10.1039/C6TC02526A.

[18] Luo H Z, Liu G D, Meng F B, Wang W H, Wu G H, Zhu X X and Jiang C B (2011) Half-metallicity and magnetic properties of half-Heusler type Mn2Sn: Ab initio predictions Physica B 406, 4245-4248. https://doi.org/10.1016/j.physb.2011.08.020.

[19] Clark S.J, Segall M.D, Pickard C.J, Hasnip P.J, Probert M.I, Refson K, Payne M.C (2005) First principles methods using CASTEP, Z. Krist. 220 567. http://dx.doi.org/10.1524/zkri.220.5.567.65075.

[20] Perdew J.P, Burke K, Ernzerhof M (1996) Phys. Rev. Lett. 77 3865. https://doi.org/10.1103/PHYSREVLETT.78.1396.

[21] Slater J.C (1936) Phys. Rev. 49, 931. https://doi.org/10.1103/PhysRev.49.931.

[22] Pauling L (1938) Phys. Rev. 54, 899. https://doi.org/10.1103/PhysRev.54.899.

[23] Guo G.Y Chu K.C Wang D.S Duan C.G (2004) Phys. Rev. B 69, 205416. https://doi.org/10.1103/PhysRevB.69.205416.

[24] Gajdoš M, Hummer K, Kresse G, Furthmüller J, Bechstedt F (2006) Phys. Rev. B 73, 045112. https://doi.org/10.1103/PhysRevB.73.045112.